# Virtual Impedance Based Stability Analysis for Direct Digital Controlled Single-Phase Grid-Connected Inverter with LCL Filter having Wide Inductance Variation

Tsai-Fu Wu, Mitradatta Misra, Ying-Yi Jhang and Chun-Yi Lin
Elegant Power Electronic Application Research Laboratory
Department of Electrical Engineering
National Tsing Hua University
Hsinchu, Taiwan
email: tfwu@ee.nthu.edu.tw

***Abstract*—In this paper an approach to adapting virtual impedance based stability analysis method for direct digital controlled grid-connected inverters with LCL filters having wide non-linear variation in inductance is presented. The non-linear time-varying inductance is due to soft-saturation characteristics of powder-iron inductor core, whose magnetic permeability varies with current. A state-space switching average model of the system is derived considering time-varying filter inductance terms. An energy-based Lyapunov function is used to show that stability of the system at any operating point is independent of the time-varying filter inductance terms. The stability is then analyzed graphically from a simplified parameterized model in s-domain using the concept of virtual impedance with filter inductance in the third dimension. Experimental results from a 5 kW single-phase grid-connected inverter implementing direct digital control based on an anhysteretic filter inductance model have shown good agreement with analytical results for various LCL parameters. The effect of hysteresis on stability behavior is further postulated and verified from the experimental results.**

***Keywords—Virtual Impedance; Stability Analysis; LCL Filter; Lyapunov; Hysteresis; Direct Digital Control;***

## I. INTRODUCTION

Non-linear variation in inductance due to powder core's soft saturation characteristics is a well-established fact [1]. Hence, passive filter design for inverter-based applications with powder core requires careful consideration [2]-[3]. Design complexity increases further with LCL filter-based applications due to the associated varying resonance frequency [4]. Although, the control complexity with LCL filters is significantly reduced by implementing direct digital control based on an anhysteretic filter inductance model [5]-[6], stability analysis is often done with nominal inductance only. The effect of non-linear filter inductance on grid-current harmonics has been investigated with single L filters [7]-[8], but to the authors' knowledge, an explicit study on stability analysis of inverters with LCL filters exhibiting non-linear and time-varying behavior has never been done before. The time-delay dependent region of stability, which is an important parameter for determining control performance with LCL filters, has not been investigated either with due consideration to nonlinear inductance. It has been shown that the region of stability is not affected by filter inductance values in single-loop current feedback based control methods [9]-[10], and stability boundary is typically derived to be one-sixth of sampling frequency. However, it is not true for controls with additional feedback based active damping mechanisms [10].

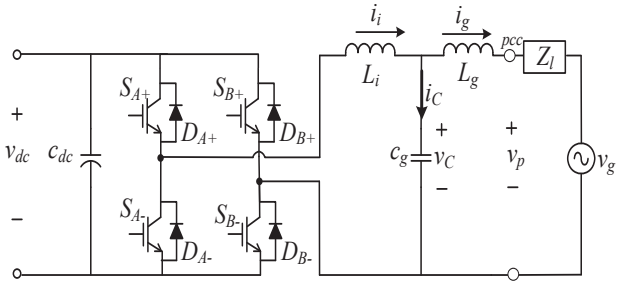


Fig.1. Single phase bidirectional inverter with an LCL filter

In this research, it will be shown that the region of stability shifts with filter inductance variation in direct digital control methods even without any additional feedback based active damping terms. A state-space average model with time-varying filter inductance terms for single-phase inverter with LCL filters, as shown in Fig. 1, will be derived first. Then, using an energy-based Lyapunov function, it will be shown that the time-varying terms do not affect the first-order time derivative of the energy function. This proves that stability can be analyzed from the corresponding simplified model only. Next, the concept of virtual impedance to determine the region of stability is applied for a known parameter bound, defined by the maximum drop in inductance. The effect of hysteresis on stability is also postulated and finally, experimental results from a 5 kW single-phase inverter with various LCL parameters are shown to verify the analytical results. The inverter prototype specifications are shown in Table I.

TABLE I. SYSTEM PARAMETERS OF INVERTER PROTOTYPE.

| Parameters | Symbol | Values | |
|---|---|---|---|
| DC-link voltage | $v_{dc}$ | 360 ~ 400 V | |
| AC output voltage | $v_{g,rms}$ | 220 V | |
| Maximum rated power | $P_{rated}$ | 5 kW | |
| Line frequency | $f_0$ | 60 Hz | |
| Switching Frequency | $f_s$ | 30 kHz | |
| ***LCL Filters*** | | **Case (a)** | **Case (b)** |
| Inverter-side Inductance | $L_i$ | 1.2 mH | |
| Filter Capacitor | $C_g$ | 5 μF | 10 μF |
| Grid-side Inductance | $L_g$ | 0.28 mH | |

## II. VIRTUAL IMPEDANCE AND STABILITY ANALYSIS

### A. Dynamic Model of Single-Phase Grid-Connected Inverter with Time-Varying LCL Filters

A dynamic model of the system shown in Fig. 1 considering bipolar operation is given by

$$\begin{bmatrix} \frac{di_i}{dt} \\ \frac{dv_c}{dt} \\ \frac{di_g}{dt} \end{bmatrix} = \begin{bmatrix} -\frac{1}{L_i}\frac{dL_i}{dt} & -\frac{1}{L_i} & 0 \\ \frac{1}{C_g} & 0 & -\frac{1}{C_g} \\ 0 & \frac{1}{L_g+L_L} & -\frac{1}{L_g+L_L}\frac{dL_g}{dt} \end{bmatrix} \begin{bmatrix} i_i \\ v_c \\ i_g \end{bmatrix} + \begin{bmatrix} \frac{2d-1}{L_i} & 0 \\ 0 & 0 \\ 0 & -\frac{1}{L_g+L_L} \end{bmatrix} \begin{bmatrix} v_{dc} \\ v_g \end{bmatrix}, \quad (1)$$

where $d$ is the duty ratio. The above model is similar to standard dynamic models, such as that presented in [11], except for the additional time-varying inductance terms. A typical time-varying inductance profile under steady-state operation is shown in Fig. 2. Since, current varies with time, inductance also varies with time, with the maximum at current zero-crossing and the minimum at current peak.

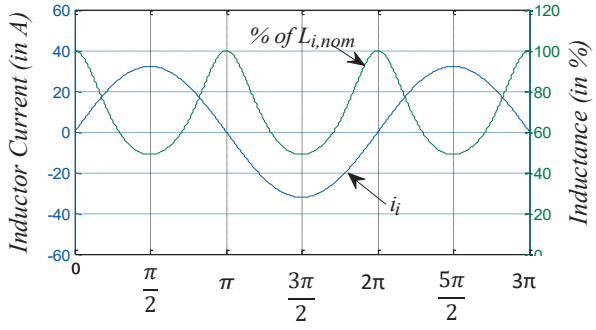


Fig. 2. A Typical Time-Varying Inductance Profile.

The time-varying inductance terms in (1) are included in the model by considering voltage across inductors $v_{Lx}$ to be of the form

$$v_{Lx} = \frac{d}{dt}(L_x i_x) = L_x \frac{di_x}{dt} + i_x \frac{dL_x}{dt}, \quad (2)$$

where subscript "$x$" is "$i$" for inverter-side inductor and "$g$" for grid-side inductor.

### B. Significance of Time-Varying Inductance Terms On Stability

The significance of time-varying inductance terms on stability could be verified from Lyapunov stability criterion [12]. The idea is to choose an energy-like Lyapunov function and check if the first-order derivative of the function depends on the time-varying terms or not. The following coordinate transformation is applied:

$$\begin{aligned} x_i &= i_i - i_i^*, \\ x_c &= v_c - v_c^*, \\ &\text{and} \\ x_g &= i_g - i_g^*, \end{aligned} \quad (3)$$

where $i_i^*$, $v_c^*$ and $i_g^*$ are the steady-state reference operation trajectories for $i_i$, $v_c$ and $i_g$ respectively. The coordinate transformation (3) allows the equilibrium point to be simplified to the origin (0, 0, 0) over the entire range of inductance variation, without affecting the result of stability analysis. Then substituting $i_i^*$, $v_c^*$ and $i_g^*$ in (1) and subtracting the resultant equation from (1), we have the dynamic model in the new coordinates as shown below:

$$\begin{bmatrix} \frac{dx_i}{dt} \\ \frac{dx_c}{dt} \\ \frac{dx_g}{dt} \end{bmatrix} = \begin{bmatrix} -\frac{1}{L_i}\frac{dL_i}{dt} & -\frac{1}{L_i} & 0 \\ \frac{1}{C_g} & 0 & -\frac{1}{C_g} \\ 0 & \frac{1}{L_g+L_L} & -\frac{1}{L_g+L_L}\frac{dL_g}{dt} \end{bmatrix} \begin{bmatrix} x_i \\ x_c \\ x_g \end{bmatrix} + \begin{bmatrix} \frac{2u}{L_i} & 0 \\ 0 & 0 \\ 0 & 0 \end{bmatrix} \begin{bmatrix} v_{dc} \\ v_g \end{bmatrix}, \quad (4)$$

where $u$ is defined as $u = d - d^*$, with $d^*$ referring to the steady-state operating trajectory for the duty ratio.

Now, a function $V(\boldsymbol{x})$, that satisfies the basic properties of global positive definiteness, *i.e.*

$$\begin{aligned} &V(0) = 0 \\ &V(\boldsymbol{x}) > 0, for\ all\ \boldsymbol{x} \neq 0 \\ &V(\boldsymbol{x}) \to \infty\ as\ \|\boldsymbol{x}\| \to \infty \end{aligned} \quad (5)$$

is defined as shown below:

$$V(x_i, x_c, x_g) = \frac{1}{2}\left(L_i^2 x_i^2 + C_g^2 x_c^2 + (L_g + L_l)^2 x_g^2\right). \quad (6)$$

The first-order time derivative of the Lyapunov function $\dot{V}(x_i, x_c, x_g)$ is typically required to be negative definite for global asymptotic stability [12]. Thus, substituting (4) in the first-order derivative of (6) and assuming constant line inductance, the expression for $\dot{V}(x_i, x_c, x_g)$ is derived to be

$$\dot{V}(x_i, x_c, x_g) = L_i x_i (2u v_{dc} - x_c) + C_g x_c (x_i - x_g) + (L_g + L_l) x_g x_c. \quad (7)$$

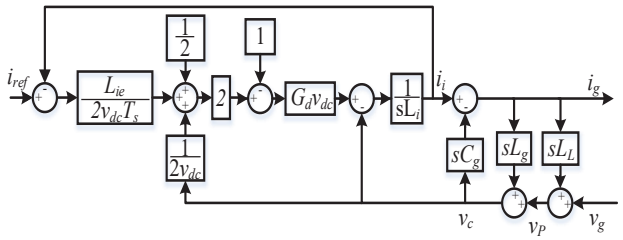

Fig. 3. Control block diagram for direct digital control.

It can be observed from (7) that $\dot{V}(x_i, x_c, x_g)$ is dependent only on the instantaneous value of the inductance at operating point, i.e. $L_i$ and $L_g$. The time-varying inductance terms in (4) eventually get canceled out in (7), thus confirming that they don't affect overall stability.

The only limitation with the above analysis is that with choice of Lyapunov function. Since, negative definiteness of (7) cannot be verified, it can be argued that (6) may not be an appropriate Lyapunov function. Nevertheless, the above conclusion regarding effect of time-varying inductance terms on stability can also be drawn intuitively. Powder-iron cores with soft saturation characteristics are typically known to have good inductance stability around the operating point [1]. And, conventional stability analysis is usually performed with the assumption of small-signal perturbations. Hence, for an instantaneous value of inductance at an operating point, the time-varying inductance terms can also be intuitively assumed to be negligible for small signal perturbations in inductor currents. Thus, a simplified dynamic model without time-varying inductance terms should be sufficient to analyze stability, albeit with different instantaneous inductance values over the entire range of allowable variation.

### C. Direct Digital Control Law

The direct digital control law for bipolar operation without any additional compensation terms as derived in [5] is given by

$$d = \frac{1}{2} + \frac{v_c}{2v_{dc}} + \frac{L_{ie}}{2v_{dc}T_s}\left(i_{ref} - i_i\right), \tag{8}$$

where $L_{ie}$ is the estimate of the inverter-side inductance from the anhysteretic filter inductance model. The corresponding control block diagram is shown in Fig. 3, where $G_d = e^{-sT_s}$ refers to one-switching cycle time delay.

### D. Virtual Impedance

The virtual impedance based analysis is typically used to determine the region of stability and gain boundary of the controller by investigating the damping due to their virtual impedance terms [10]. The underlying principle is that, virtual resistance due to controller at the effective resonance frequency should be positive for stability. Since, the direct digital control uses an estimate of filter inductance as the controller gain, virtual impedance based analysis can be a helpful tool in choosing an appropriate inductor core. The maximum allowable drop in inductance beyond which the control can become unstable is determined and the corresponding inductor core is selected.

It can be seen from (8) and the block diagram in Fig. 3 that, the direct digital control is essentially an inverter-side inductor current $i_i$ feedback based control with an additional filter capacitor voltage $v_c$ feedforward. This is unlike single-loop $i_i$ current feedback based control which could be represented as a single impedance in series with $L_i$ [10]. Hence, $i_i$ is first split into $i_g$ and $i_c$ feedbacks. The equivalent block diagram is shown in Fig. 4(a). Then applying simple rules for block diagram reduction, found in classical control theory textbooks [13], $i_g$ and $i_c$ feedbacks are represented as $v_c$ feedback, shown in Fig. 4(b). The $v_c$ feedback terms from Fig. 4(b) along with the $v_c$ feedforward term are further reduced to equivalent virtual impedance terms in parallel with $C_g$, shown in Fig. 4(c). The virtual impedance terms are derived by multiplying the gains along the control path and given by expressions in (9). $Y_{ic}$ and $Y_{ig}$ represent the virtual admittance due to equivalent $i_c$ and $i_g$ current feedback, while $Y_{vc}$ represents the virtual admittance due to $v_c$ feedforward in (9). Finally, a single virtual impedance $Z_v$ in parallel with the filter capacitor $C_g$ is derived, as shown in Fig. 4(d). The total virtual impedance can be further represented as a virtual resistor $R_v$ in parallel with a virtual capacitor $C_v$. The corresponding expressions derived in frequency domain are given by (10) and (11).

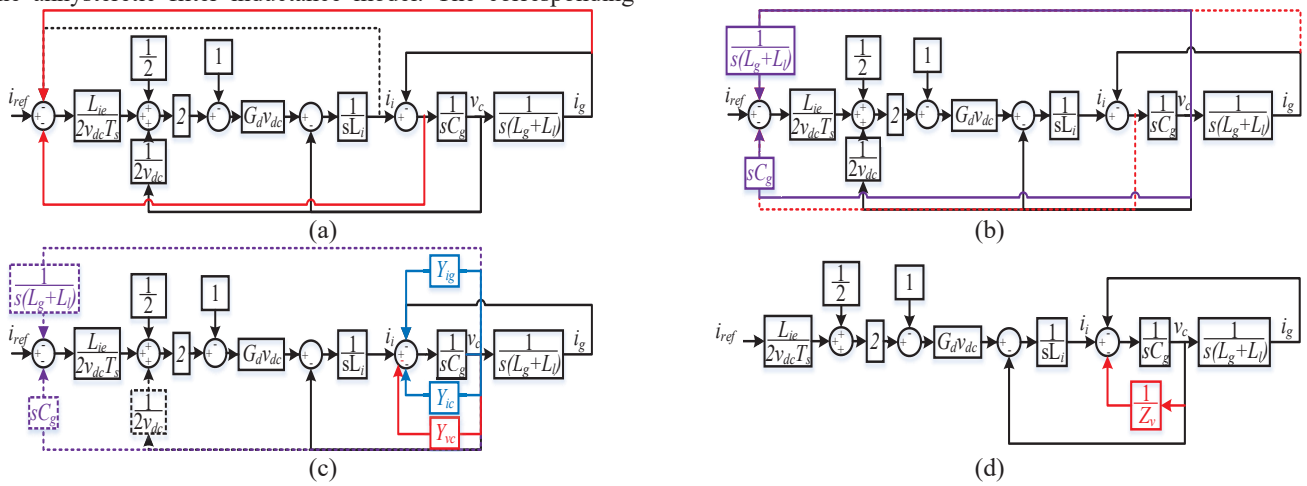

Fig. 4. Block diagram reduction for direct digital control to derive the virtual impedance terms.

$$Y_{ic} = \frac{G_d L_{ie} C_g f_s}{L_i},$$
$$Y_{ig} = \frac{G_d L_{ie} f_s}{s^2 L_i (L_g + L_l)}, \quad (9)$$
$$Y_{vc} = -\frac{G_d}{s L_i},$$

$$R_v = \frac{(2\pi f)^2 L_i (L_g + L_l)}{\left\{\begin{array}{c} -f_s \cos\left(\frac{2\pi f}{f_s}\right) L_{ie} + \\ (2\pi f)^2 f_s \cos\left(\frac{2\pi f}{f_s}\right) L_{ie}(L_g + L_l) C_g + \\ (2\pi f) \sin\left(\frac{2\pi f}{f_s}\right)(L_g + L_l) \end{array}\right\}} \quad (10)$$

and

$$C_v = \frac{\left\{\begin{array}{c} f_s \sin\left(\frac{2\pi f}{f_s}\right) L_{ie} - \\ (2\pi f)^2 f_s \sin\left(\frac{2\pi f}{f_s}\right) L_{ie}(L_g + L_l) C_g + \\ (2\pi f) \cos\left(\frac{2\pi f}{f_s}\right)(L_g + L_l) \end{array}\right\}}{(2\pi f)^3 L_i (L_g + L_l)}. \quad (11)$$

The resonant frequency would shift because of the virtual capacitance $C_v$ and this effective resonant frequency $f'_{res}$ due to $L_i$, $C_g$, $L_g$ and $C_v$ is given by expression (12).

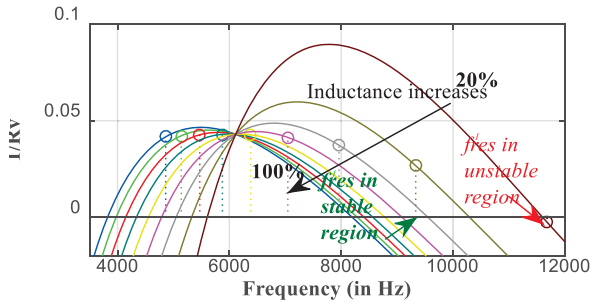


(a)

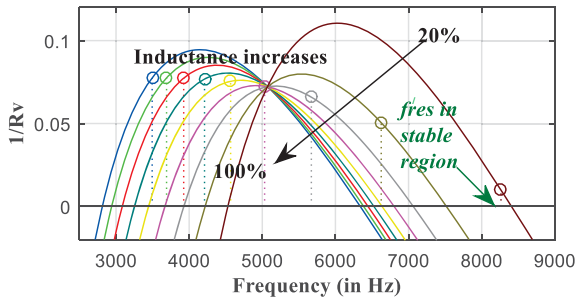


(b)

Fig. 5. Virtual conductance plots for inductance variation between 20 and 100% of nominal value
$L_i$ = 1.2 mH, $L_g$ = 0.28 mH, (a) $C_g$ = 5 µF and (b) $C_g$ = 10 µF

$$f'_{res} = \frac{1}{2\pi}\sqrt{\frac{L_i + (L_g + L_l)}{L_i (L_g + L_l)(C_g + C_v)}}. \quad (12)$$

Now, stability is analyzed by plotting the virtual conductance $1/R_v$ for the complete range of inductance variation and frequency, and then tracing the value of $1/R_v$ calculated at $f'_{res}$. A two-dimensional projection of the plot along the $(1/R_v)$-$f$ plane for the two different sets of LCL parameters, ***Case(a)*** and ***Case(b)***, as specified in Table I are shown in Fig. 5. It can be observed that a virtual conductance plot at nominal value of inductance (plot in BLUE) would have predicted stability for both cases. However, when drawn over the entire range of inductance variation, it is observed that Case (a) has the potential to be unstable when inductance is at 20% of nominal value, Fig. 5(a), while Case (b) remains stable throughout, Fig. 5(b), (plot in BROWN). This clearly highlights the importance of checking the trace of virtual conductance at effective resonant frequency over the entire range of inductance variation for complete picture of stability. Hence, while choosing the core for filter inductors in Case(a), it must be ensured that filter inductance does not drop below 30~40% of nominal value at peak inductor current.

### *E. Effect of Hysteresis*

The plots in Fig. 5 are drawn assuming that the estimated value of inductance from the anhysteretic model is exactly same as the actual value of inductance. However, due to hysteresis effect, magnetic permeability and hence inductance would not match with the anhysteretic value. In fact, during line cycle magnetization (*i.e.* rising current in positive and negative half cycle), the estimated value of inductance would be higher than the actual value and during line cycle demagnetization (i.e. falling current in positive and negative half cycle), the estimated value of inductance would be smaller than the actual value, as observed in a typical hysteresis curve shown in Fig. 6. Thus, the potential for $f'_{res}$ to move into region where $R_v$ is negative is higher during magnetization than during demagnetization in the line cycle. The virtual conductance plots

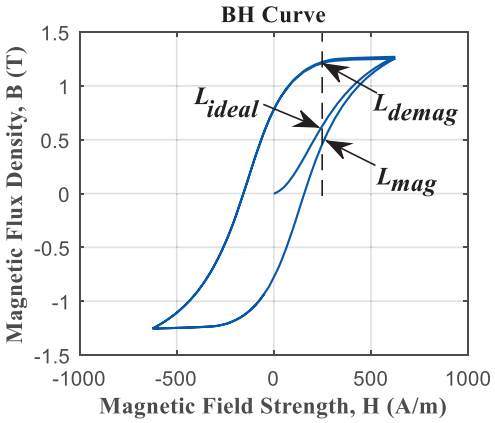


Fig. 6. Difference in estimated inductance and actual inductance due to hysteresis

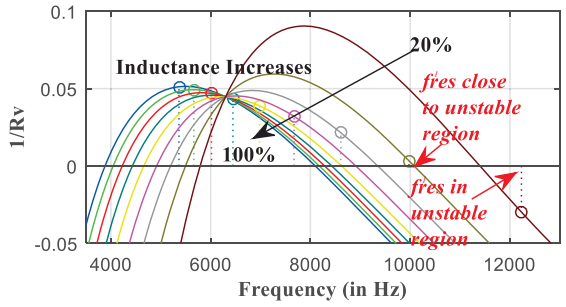


(a)

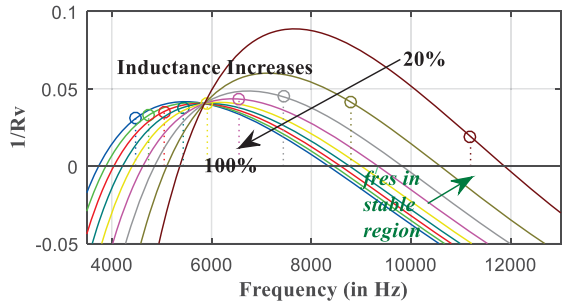


(b)

Fig. 7. Virtual conductance plots for LCL parameters of Case (a) with estimated inductance mismatch during (a) magnetization and (b) demagnetization

corresponding to Case (a) are redrawn considering the effect of hysteresis in Fig. 7. It can now be observed that, due to the mismatch in estimated inductance from anhysteretic model, $f'_{res}$ moves closer to the unstable region at even higher inductance value during magnetization, Fig. 7(a), while it moves into the stable region for the entire range of operation during demagnetization, Fig. 7(b). Another point to note here is that since the inductance keeps changing over one cycle, there is always a possibility that the oscillations are not sustained over the entire line cycle.

### *F. Limitations of Virtual Impedance-based Stability Analysis*

Virtual impedance-based stability analysis can pretty accurately predict absolute stability under wide inductance variation. However, it cannot provide any measure of relative stability, *i.e.* stability margins like phase and gain margins. This limitation is similar to that of conventional root locus method. It can only assist in estimating the range of inductance variation beyond which the control would become unstable. Other frequency response plots like bode or Nyquist would still be necessary to complement the virtual impedance method.

## III. Experimental Results

The stability analysis done in the previous section along with the effect of hysteresis is experimentally verified from a 5 kW grid-connected inverter operated in bipolar mode with specifications according to Table I. The inductor cores are chosen such that drop in inductance is around 25% at rated current. The corresponding inverter-side inductor current $i_i$, grid-side inductor current $i_g$ along with voltage at point-of-

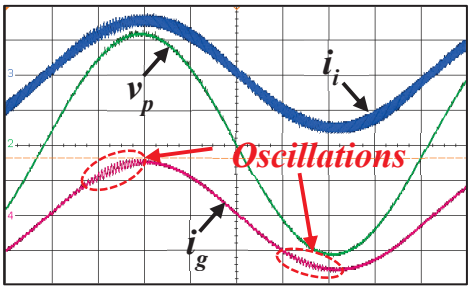


(a)

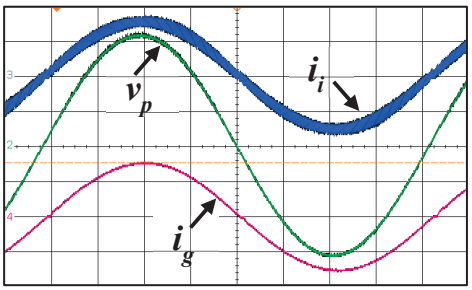


(b)

*($i_i$ and $i_g$: 20 A/div; $v_p$: 100 V/div; time:2 ms/div)*

Fig. 8. Steady State Waveforms at rated current with LCL parameters as $L_i$ = 1.2 mH, $L_g$ = 0.28 mH, (a) $C_g$ = 5 µF and (b) $C_g$ = 10 µF

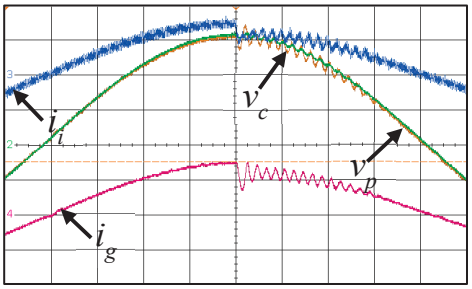


(a)

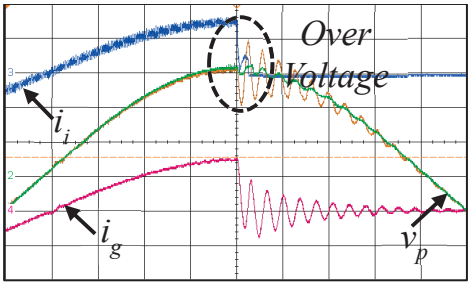


(b)

*($i_i$ and $i_g$: 20 A/div; $v_c$ and $v_p$: 100 V/div; time:1 ms/div)*

Fig. 9. Transient State Waveforms with LCL parameters as $L_i$ = 1.2 mH, $L_g$ = 0.28 mH and $C_g$ = 10 µF during step-down near the peak for (a) 5 kW to 4 kW and (b) 5 kW to 1 kW

common coupling $v_p$ are shown in Fig. 8. Steady-state oscillations are observed for Case (a), Fig. 8(a) while not for Case (b), Fig. 8(b). This is in good agreement with stability analysis done in the previous section. It is also observed in Fig. 8(a) that the oscillations observed during line cycle magnetization are damped out during line cycle demagnetization, which confirms the effect of hysteresis on stability. The LCL parameters for Case (b) are used to perform step-down operations so as to verify the transient-state stability. As can be observed from Fig. 9 (a), the undershoot during a step-down from 5 kW to 4 kW did not cause capacitor voltage $v_c$ overshoot. However, during a step-down from 5 kW to 1 kW, the system went into protection due to resulting capacitor voltage $v_c$ overshoot, shown in Fig. 9 (b). With a higher protection limit for $v_c$, the system could have eventually settled down, but would have required longer settling time. This emphasizes the limitation of virtual impedance-based stability analysis in estimating relative stability measures.

## IV. Conclusions

Stability analysis with only nominal values of LCL parameters may not provide an accurate picture of stability for inductors exhibiting wide variation from their nominal value due to the core's permeability. Moreover, direct digital control method based on anhysteretic inductance model can exhibit instability due to mismatch in estimated inductance from hysteresis effect. Direct digital control methods inherently being an inverter-current feedback based control with terminal voltage feedforward, the stability behavior would also be different from conventional single-loop current feedback based controls. Hence, a virtual impedance based stability analysis method adapted to direct digital control based on anhysteretic inductance model for wide variation in filter inductance has been presented in this paper. The applicability of the method for small-signal stability, even in the presence of time-varying inductance terms in the dynamic model, has been intuitively and mathematically verified through an energy-based Lyapunov function. And then the virtual impedance terms have been derived. The analytical results from virtual conductance plots have been experimentally verified. The effect of hysteresis on stability has also been postulated and confirmed from experimental results. Such an analysis is important for control engineers to identify the maximum drop in inductance that could be allowed without affecting stability. It can also help in determining the necessary adjustments to the inductance model for dealing with hysteresis effect. Limitations of the analysis method in predicting relative measure of stability has been discussed and experimentally verified.

## References


[1] M. A. Swihart, "Inductor cores–material and shape choices," *Magnetics-www. mag-inc. com*, 2004.

[2] S. Jayalath, D. Ongayo, and M. Hanif, "Modelling powder core inductors for passive filters in inverters using finite element analysis," *Electronics Letters*, vol. 53, no. 3, pp. 179–181, 2017.

[3] Y. Liu, H. A. Mantooth, J. C. Balda, and C. Farnell, "Realization of high-current variable AC filter inductors using silicon iron powder magnetic core," in *2017 IEEE Applied Power Electronics Conference and Exposition (APEC)*, March 2017, pp. 855–860.

[4] T. F. Wu, M. Misra, L. C. Lin, and C. W. Hsu, "An improved resonant frequency based systematic LCL filter design method for grid-connected inverter," *IEEE Transactions on Industrial Electronics*, vol. 64, no. 8, pp. 6412–6421, Aug 2017.

[5] T. F. Wu, L. C. Lin, N. Yao, Y. K. Chen, and Y. C. Chang, "Extended application of D-Σ digital control to a single-phase bidirectional inverter with an LCL filter," *IEEE Transactions on Power Electronics*, vol. 30, no. 7, pp. 3903–3911, July 2015.

[6] T. F. Wu, M. Misra, L. C. Lin, and Y. H. Huang, "A modified division-summation digital control for grid-connected inverter with wide inductance variation of LCL filter," in *2017 IEEE Applied Power Electronics Conference and Exposition (APEC)*, March 2017, pp. 2781–2787.

[7] R. A. Mastromauro, M. Liserre, and A. Dell'Aquila, "Study of the effects of inductor nonlinear behavior on the performance of current controllers for single-phase PV grid converters," *IEEE Transactions on Industrial Electronics*, vol. 55, no. 5, pp. 2043–2052, May 2008.

[8] J. Viinamäki, J. Jokipii, and T. Suntio, "Effect of inductor saturation on the harmonic currents of grid-connected three-phase VSI in PV application," in *2015 9th International Conference on Power Electronics and ECCE Asia (ICPE-ECCE Asia)*, June 2015, pp. 1209–1216.

[9] J. Wang, J. D. Yan, L. Jiang, and J. Zou, "Delay-dependent stability of single-loop controlled grid-connected inverters with LCL filters," *IEEE Transactions on Power Electronics*, vol. 31, no. 1, pp. 743–757, Jan 2016.

[10] J. Wang and J. D. Yan, "Using virtual impedance to analyze the stability of LCL-filtered grid-connected inverters," in *2015 IEEE International Conference on Industrial Technology (ICIT)*, March 2015, pp. 1220–1225.

[11] S. Eren, M. Pahlevaninezhad, A. Bakhshai, and P. K. Jain, "Composite nonlinear feedback control and stability analysis of a grid-connected voltage source inverter with LCL filter," *IEEE Transactions on Industrial Electronics*, vol. 60, no. 11, pp. 5059–5074, Nov 2013.

[12] H. Khalil, *Nonlinear Systems*, 3rd Edition. Prentice Hall, 2002.

[13] Nagrath, J., and Gopal, M., *Control System Engineering*, 5th Edition, New Age International Publishers, 2007.